JACS
JOURNAL OF THE AMERICAN CHEMICAL SOCIETY

COMMUNICATION

pubs.acs.org/JACS

Container Effect in Nanocasting Synthesis of Mesoporous Metal Oxides

Xiaohong Sun,[†,⊥] Yifeng Shi,[*,‡] Peng Zhang,[§] Chunming Zheng,[†] Xinyue Zheng,[‡] Fan Zhang,[§] Yichi Zhang,[§] Naijia Guan,[*,†] Dongyuan Zhao,[∥] and Galen D. Stucky[*,§]

[†]Key Laboratory of Advanced Energy Materials Chemistry, College of Chemistry, Nankai University, Tianjin 300071, China

[‡]College of Material, Chemistry and Chemical Engineering, Hangzhou Normal University, Hangzhou 310036, China

[§]Department of Chemistry & Biochemistry, University of California, Santa Barbara, California 93106, United States

[∥]Department of Chemistry, Fudan University, Shanghai 200433, China

[⊥]Key Lab of Advanced Ceramics and Machining Technology, School of Materials Science and Engineering, Tianjin University, Tianjin 300072, China

Supporting Information

ABSTRACT: We report a general reaction container effect in the nanocasting synthesis of mesoporous metal oxides. The size and shape of the container body in conjunction with simply modifying the container opening accessibility can be used to control the escape rate of water and other gas-phase byproducts in the calcination process, and subsequently affect the nanocrystal growth of the materials inside the mesopore space of the template. In this way, the particle size, mesostructure ordering, and crystallinity of the final product can be systemically controlled. The container effect also explain some of the problems with reproducibility in previously reported results.

Ordered mesoporous materials have been extensively investigated in the last two decades because of their uniform pore sizes, tunable pore structures, ease of functionalization, and high surface areas.[1] Beyond the most-investigated silica- and carbon-based materials, metal oxides have attracted considerable interest due to their more diverse electronic functionality, which includes photocatalytic activities, semiconductor characteristics, and magnetic properties.[2] Mesoporous metal oxides can be directly synthesized by the cooperative assembly of inorganic metal precursors and organic surfactants via a sol−gel process.[3] However, their applications have been limited by poor mesoscale phase separation due to framework crystallization, which leads to loss of mesostructure definition. Nanocasting is an efficient approach for synthesis of highly ordered crystalline mesoporous materials, because the hard templates provide stable supports for high-temperature crystallization.[4] A large number of mesoporous metal oxides have been successfully prepared by using the nanocasting method.[5]

Metal nitrates are the most commonly used precursors in nanocasting because they can be readily impregnated into the templates and then in situ converted to corresponding metal oxides. Distinct volume shrinkage occurs during the conversion due to the weight loss and density increase. Theoretical estimations based on the chemical reaction equations and bulk density data reveal that only 5−15% of the pore space is occupied by metal oxides after the conversion, even if the mesoporous template is 100% filled with metal nitrates at the beginning (see Supporting Information (SI) Table S1).[5b,6] Consequently, the final products possess much smaller particle sizes than their mother templates. Although the particle sizes of the mother templates may be as large as several hundred micrometers, the nanocast metal oxide products generally have particle sizes of 50−300 nm, which are not desirable for separation and unsuitable for some applications.[7] Multicycle nanocasting does not greatly help to increase the size of the nanocast mesoporous metal oxide particles.[8] To our knowledge, no effective method has been reported to sufficiently control the product particle size over a wide range in the nanocasting of metal oxides.

Here, for the nanocasting of metal oxides, we report how the shape and size of the sample container body, in conjunction with the container opening accessibility, can be easily utilized to systematically control the particle size from <50 nm to several micrometers, as well as the crystallinity and mesostructure ordering. The proposed strategy is to use the sample container and restrict the sample opening to control the escape rate of water and other gas-phase byproducts in the calcination process. This determines the crystal growth behavior of the materials and leads to structural differences of the final products. Some previously reported inconsistent results can be explained by this container effect. Because of the increasing interest in its use as a magnetic material,[9] iron oxide is used as an example for the demonstration. The container effect in the syntheses of ordered mesoporous NiO, In_2O_3, Co_3O_4, Cr_2O_3, and CeO_2 is also described.

Mesoporous silica KIT-6 with particle sizes from 20 to 300 μm was synthesized according to the literature and used as a template.[10] $Fe(NO_3)_3 \cdot 9H_2O$ was used as metal precursor and loaded into the mesopores of KIT-6 via a so-called "two solvents method".[11] The obtained precursor@silica intermediate was then calcined from 25 to 600 °C with a ramp of 1 °C/min in a Muffle furnace, where $Fe(NO_3)_3 \cdot 9H_2O$ was converted to Fe_2O_3 upon the calcination. The silica template was removed with a 2 M NaOH aqueous solution. Two sets of samples were prepared from the same batch and subjected to the same calcination procedure, but different sample containers were used during the calcination: Sample mFe_2O_3-C was synthesized by loading the intermediate in a glass bottle covered with a glass slide, while

Received: June 29, 2011
Published: August 23, 2011

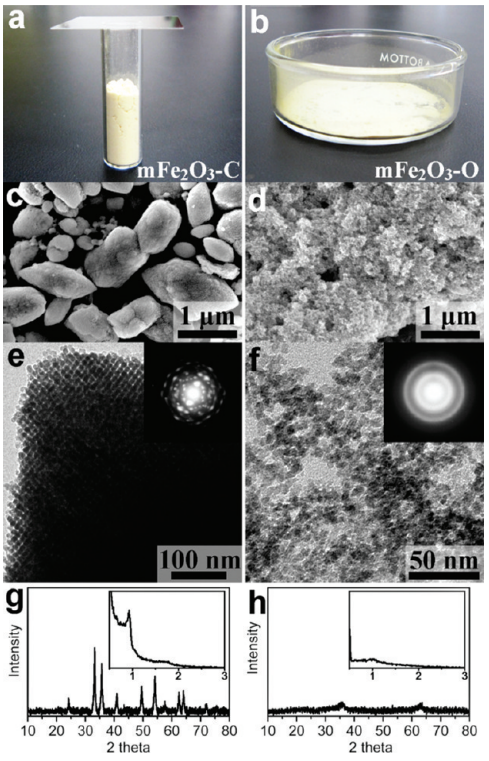

Figure 1. SEM images (c, d), TEM images (e, f), and XRD patterns (g, h) of two mesoporous Fe_2O_3 samples, which were synthesized in the same way except for the use of different sample containers (a, b). The products synthesized in the quasi-sealed container possess large particle size and highly ordered mesoporous structure (a, c, e, g); the products synthesized in the open Petri dish are nearly amorphous isolated nanoparticles (b, d, f, h).

sample mFe_2O_3-O was prepared by spreading the intermediate in a Petri dish without any cover, as shown in Figure 1a,b.

Scanning electron microscopy (SEM) observations reveal that mFe_2O_3-C possesses a large particle size in the range of 300−2000 nm (Figure 1c). All particles possess a highly ordered mesostructure as revealed by high-resolution SEM (SI Figure S2) and transmission electron microscopy (TEM; Figure 1e) images. The mesostructure regularity is also confirmed by the intense and sharp diffraction peaks observed in the small-angle X-ray diffraction (XRD) pattern (Figure 1g inset). Well-defined diffraction peaks can be clearly observed in the wide-angle XRD pattern (Figure 1g), indicating the crystalline nature of mFe_2O_3-C. The peaks can be indexed as a rhombohedral phase of Fe_2O_3 (JCPDS: 33-0664), α-Fe_2O_3. Nitrogen sorption isotherms of the mFe_2O_3-C sample show typical type-IV isotherms with a clear step at p/p_0 of 0.6−0.8, suggesting the presence of uniform mesoporosity (SI Figure S3). The corresponding pore size distribution curve, calculated from the adsorption branch by the Barrett−Joyner−Halenda method, shows that the mean pore size is in the range of 3−11 nm. All these results confirm that a highly ordered crystalline mesoporous Fe_2O_3 material with particle size up to 2 μm is obtained.

Sample mFe_2O_3-O shows distinctly different results from mFe_2O_3-C in particle size, crystallinity, and mesostructure ordering. SEM (Figure 1d) and TEM (Figure 1f) images both illustrate that mFe_2O_3-O is composed of isolated nanoparticles (NPs) without long-range mesostructure ordering. Although the particle shape is not uniform, its diameter is always ∼7 nm, consistent with the mesopore diameter of the template. This feature suggests that these NPs are formed inside the mesopore but do not assemble together as in the case of mFe_2O_3-C. The wide-angle XRD pattern of mFe_2O_3-O (Figure 1h) only shows two weak and broad diffraction peaks, further suggesting a small particle size and less crystallinity. N_2 sorption analyses (SI Figure S3) show that mFe_2O_3-O possesses a broad pore size distribution from 5 to 60 nm, probably caused by particle aggregation. The distinct structural differences between mFe_2O_3-C and mFe_2O_3-O clearly demonstrate that the container can significantly affect the particle size, mesostructure regularity, and crystallinity of the products.

Mesoporous Co_3O_4, NiO, In_2O_3, Mn_3O_4, CeO_2, and Cr_2O_3 have also been synthesized previously by using metal nitrates as precursors via nanocasting. We synthesized these samples using different sample containers (SI Figures S4−S9), and a similar container effect is observed in all the tests as in the case of Fe_2O_3. Highly ordered mesoporous metal oxides with large particle sizes are obtained when they are calcined in quasi-sealed small glass bottles. In contrast, products synthesized in open Petri dishes give small NPs with poor mesostructural ordering. It should be noted that, in some cases, the small NPs synthesized in the open system still possess relatively high crystallinity. This may be because the calcination temperature (600 °C) is high enough to cause sintering for these materials.

We do not observe similar container effects in the synthesis of nanocast MoO_2 and WO_3, for which phosphomolybdic acid and phosphotungstic acid are, respectively, used as precursors. This suggests that the mechanism behind the container effect is related to the metal nitrate precursors. We tested the effect of atmosphere in the nanocasting of Fe_2O_3 in a tube furnace. With a large gas flow passing through the reaction tube, the products obtained are disordered NPs (SI Figure S10), irrespective of the gas that is used. Calcination in vacuum leads to similar results, suggesting that if the gas phase byproducts are removed, metal nitrate tends to form isolated NPs rather than large mesostructured domains.

The effect of calcination temperature was examined for two sets of mFe_2O_3-C and mFe_2O_3-O samples by decreasing the calcination temperature from 600 to 100 °C in steps of 100 °C. It is found that the crystallinity is mainly determined by the sample container and not by the calcination temperature (SI Figure S11). When the Petri dish was used as a container, all samples showed nearly amorphous phases. On the other hand, well crystallized Fe_2O_3 was formed at a fairly low temperature of 200 °C in the case of mFe_2O_3-C. This result, combined with the tube furnace experiments, suggests that the decomposition of nitrate precursors at 100−200 °C is the key step.

The decomposition of $Fe(NO_3)_3 \cdot 9H_2O$ without the silica template was carefully investigated in a deep glass bottle and in an open Petri dish for comparison. In the open system, iron nitrate melted at ∼50 °C. Water evaporated with increasing temperature, and a solid dark-brown intermediate was formed before the temperature reached 100 °C. When the temperature was gradually increased to 200 °C, the sample turned red-brown. The XRD patterns of the solids are similar to those of mFe_2O_3-O. In the quasi-sealed system, no distinct water evaporation was observed until the temperature reached ∼145 °C, confirmed by the almost unchanged liquid level. However, the top void space of the container was full of brown gas, indicating the initiation of iron nitrate decomposition. The samples treated at 160 and 180 °C were mixtures of a dark-brown liquid and some red solid precipitates. XRD characterization shows that the red precipitates are highly crystallized α-Fe_2O_3, indicating that crystalline Fe_2O_3 can be directly formed from a bulk liquid phase precursor (SI Figure S12). Red solid

dx.doi.org/10.1021/ja2060512 |J. Am. Chem. Soc. 2011, 133, 14542–14545

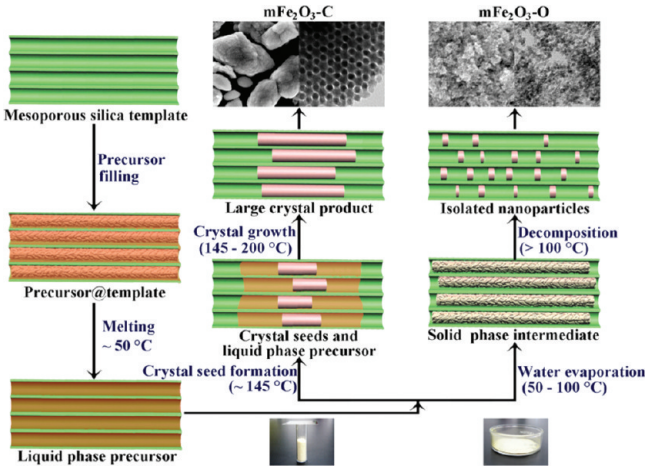

Figure 2. Scheme of the proposed mechanism for the container effect in the nanocasting synthesis of mesoporous Fe_2O_3.

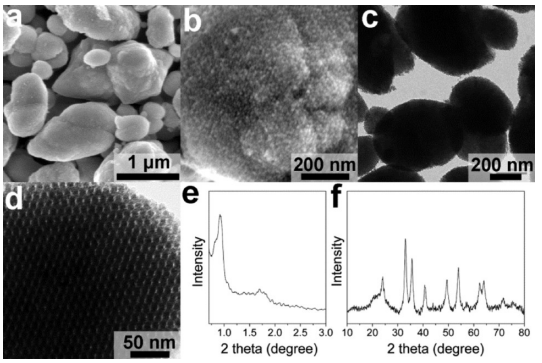

Figure 3. (a, b) SEM images, (c, d) TEM images, and (e, f) XRD patterns of mesoporous crystalline Fe_2O_3 synthesized at 150 °C.

powder α-Fe_2O_3 without any residual liquid was obtained when the temperature reached 200 °C. Thermogravimetric analysis (TGA) also shows that water is vaporized in the first step, and nitrate decomposition follows that event, if iron nitrate is heated in an open crucible, causing two clearly separated weight loss steps in its TGA curve (SI Figure S13). However, if iron nitrate is heated in a covered crucible, the water evaporation is significantly delayed to a higher temperature and only one weight loss step is recorded, confirming that the decomposition of $Fe(NO_3)_3$ occurs before water is vaporized in this case (Figure S13).

Based on these observations, we propose a direct liquid-to-solid conversion mechanism to explain the container effect in nanocasting of ordered mesoporous Fe_2O_3 (Figure 2). In a quasi-sealed container, $Fe(NO_3)_3 \cdot 9H_2O$, loaded inside the mesopores of silica template, first melts at ~50 °C. The quasi-sealed container prevents fast water evaporation and keeps the precursor in a liquid form until it reaches the decomposition temperature of iron nitrate. Then Fe_2O_3 crystal seeds are precipitated directly from the liquid precursor solution. Nitrogen oxides are released as byproducts, as evidenced by the brown gas inside the container. Nitrogen oxides can react with the residual water to form nitric or nitrous acid, which keeps the residual solution in an acid condition. If the acid is too strong, the formed Fe_2O_3 can redissolve and be converted back to iron nitrate. Quasi-equilibrium between the formation and dissolving of Fe_2O_3 occurs inside the mesopore space. The slow escape of water and nitrogen oxides from the container drives the equilibrium to Fe_2O_3 crystal growth direction during the calcination. In this way, the Fe_2O_3 crystal directly grows inside the aqueous precursor solution, which facilitates the formation of large particles. In contrast, when an open Petri dish is used as container, crystal water is rapidly evaporated to the open space after $Fe(NO_3)_3 \cdot 9H_2O$ melts, which causes solidification of the precursors before their decomposition. The solid-to-solid conversion inhibits the long-distance transportation of the iron species and thus only isolated NPs are formed inside the mesopore channels. In short, the container structure configuration influences the escape rate of water and nitrogen oxide byproducts, which affects the crystal growth behavior and hence the structure of the final products.

Besides the sample container, the configuration of the furnaces may also affect the synthesis, since when an open container is used during calcination, the entire chamber of the furnace can be regarded as the true container. In this case, if the furnace only has a small and nearly sealed chamber, highly ordered crystalline mesoporous metal oxide can be obtained even when an uncovered Petri dish is used. This is especially true when a large amount of the intermediate is calcined inside the chamber at the same time. On the other hand, if only a small amount of intermediate is loaded in an open crucible and calcined in a furnace with large size chamber, it is quite difficult to produce large particle size samples. In addition, smoke tubes will make the furnace chamber a much more open system, leading to a smaller particle size product with disordered mesostructure. This is quite similar to the significant microstructure differences observed between zeolites prepared by "deep bed" and "shallow bed" calcinations.[12] The container effect and the deep/shallow bed effect both seem to be due to the influence of container structure on the escape rate of gaseous byproducts.

Some advantages for the synthesis of mesoporous metal oxides stem from this effect. One is low-temperature synthesis. As shown in Figure S11, crystalline Fe_2O_3 products can be obtained at 200 °C. We further found that heating the $Fe(NO_3)_3 \cdot 9H_2O$@KIT-6 intermediate to 150 °C for 10 h could efficiently produce highly ordered crystalline mesoporous Fe_2O_3 (Figure 3). To the best of our knowledge, no ordered mesoporous crystalline transition metal oxide has been synthesized at such a low temperature, which means that the fabrication energy cost and equipment investment can be greatly reduced.

The second advantage is that the product particle size can be systematically controlled over a wide range, from <50 nm to several micrometers. Two pathways were successfully established. For the first pathway, the water escape rate is controlled by putting glass strips over the Petri dish with different coverage. For example, the average particle sizes of mesoporous In_2O_3 can be tuned from the micrometer size range to <100 nm in size when the Petri dishes are covered with glass strips with 100, 66, 33, and 0% coverage (Figure 4a−d and SI Figure S14). For the second pathway, the container volume is the primary control parameter. During calcination, the entire container is saturated with water vapor, which comes from the precursor solution and reduction of the water content of the precursor. Therefore, the container volume can be utilized to tune the residual water amount within the inner pore space of the template, and thus be used to control the crystal growth process. For example, when 1.0 g of iron nitrate@KIT-6 intermediate is calcined in glass bottles with volumes of 1.5, 20, 75, 480, 700, and 1200 mL, the particle sizes of the mesoporous Fe_2O_3 products can be systemically tuned from >1 μm to <50 nm (Figure 4e−p). In addition, by utilizing monolithic mesoporous silica (1−5 mm) as a hard template

dx.doi.org/10.1021/ja2060512 |J. Am. Chem. Soc. 2011, 133, 14542–14545

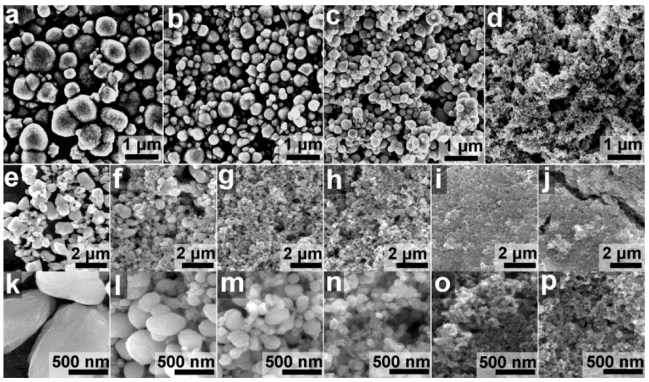

Figure 4. SEM images of the mesoporous In_2O_3 with different particle sizes synthesized in a Petri dish with (a) 100%, (b) 66%, (c) 33%, and (d) 0% glass strip coverage on its top. SEM images of the mesoporous Fe_2O_3 with different particle sizes synthesized from the same batch of intermediate but using containers with different volume: (e, k) 1.5, (f, l) 20, (g, m) 75, (h, n) 480, (i, o) 700, and (j, p) 1200 mL.

and a small glass bottle as the container, the particle sizes of some mesoporous Fe_2O_3 products are >200 μm (SI Figure S15). Such a wide range of particle size control has not been previously achieved for the nanocasting of mesoporous metal oxides.

As discussed above, the sample container, and sometimes the calcination furnace as well, have a significant effect on the particle size, mesostructural regularity, and even crystallinity of the nanocast mesoporous metal oxides. These considerations have been ignored for a long time. We believe that they are largely responsible for many of the problems in reproducing previous literature results, since different containers and furnaces were used by different groups and their configuration details have not been included in almost all the published reports. Mesoporous Fe_2O_3 is an important example. Tian et al. reported the first nanocasting of mesoporous Fe_2O_3, but the products possessed poor crystallinity and mesostructural regularity.[5c] A second nanocasting cycle was carried out to increase the mesostructure regularity by adding more iron oxide to glue together the previously formed NPs. The calcination temperatures in the first second cycles were set at 350 and 600 °C, respectively. The final products still possessed nanocrystalline nature with extensive amorphous domains and a less ordered mesostructure. Later, Jiao et al.[5d] reported a similar synthesis of mesoporous Fe_2O_3, using a similar procedure to that described by Tian et al. Interestingly, highly ordered mesoporous Fe_2O_3 with a well crystallized framework was obtained by directly heating the $Fe(NO_3)_3 \cdot 9H_2O$@KIT-6 intermediate to 600 °C without the second nanocasting cycle described in Jiao's report.[5d] Until now, no detailed reason has been provided to explain why such a small change in calcination temperature programming led to totally different products. We reproduced those two syntheses and took the container effect into account; we found that, by using a small quasi-sealed glass bottle as the container, we could synthesize highly ordered mesoporous crystalline Fe_2O_3 materials by following both Jiao's and Tian's calcination programs, as demonstrated in Figure 1 and SI Figure S16, respectively. We conclude that inconsistent results can result from the container effect and the procedures used in the synthesis should be carefully reported.

In summary, a significant container effect in the nanocasting synthesis of mesoporous metal oxides is demonstrated. It can be ascribed to the influence of the container on the escape rate of water and nitrogen oxide byproducts, which in turn affects the structure of final product. By utilizing this effect, highly ordered mesoporous crystalline metal oxides Fe_2O_3 can be synthesized at a temperature as low as 150 °C, and the particle size of the replica can be systematically controlled from several nanometers to several hundred micrometers. We believe that this effect is responsible for some inconsistent previously published results from different groups, and therefore, the details of the calcination process and apparatus configuration should be carefully considered in all future relevant research.

■ ASSOCIATED CONTENT

Supporting Information. Experimental details and characterization data. This material is available free of charge via the Internet at http://pubs.acs.org.

■ AUTHOR INFORMATION

Corresponding Author
stucky@chem.ucsb.edu; guannj@nankai.edu.cn; yfshi@hznu.edu.cn

■ ACKNOWLEDGMENT

This work was supported by the DOE-funded Center on Energy Efficient Materials (CEEM) at UCSB (DE-SC0001009), the National Science Foundation (DMR-0805148), the National Basic Research Program of China (2009CB623502), the State Scholarship Fund of China Scholarship Council (2008620020), the 863 Research Program of China (2009AA033701), Zhejiang Provincial NSFC (Y4110369), and Key Project of Chinese Ministry of Education (211066).

■ REFERENCES

(1) (a) Davis, M. E. *Nature* **2002**, *417*, 813. (b) Hartmann, M. *Chem. Mater.* **2005**, *17*, 4577. (c) Sayari, A.; Hamoudi, S. *Chem. Mater.* **2001**, *13*, 3151. (d) Schuth, F.; Schmidt, W. *Adv. Mater.* **2002**, *14*, 629.

(2) (a) Sayari, A.; Liu, P. *Microporous Mater.* **1997**, *12*, 149. (b) Schuth, F. *Chem. Mater.* **2001**, *13*, 3184. (c) Yu, C. Z.; Tian, B. Z.; Zhao, D. Y. *Curr. Opin. Solid State Mater. Sci.* **2003**, *7*, 191.

(3) (a) Yang, P. D.; Zhao, D. Y.; Margolese, D. I.; Chmelka, B. F.; Stucky, G. D. *Nature* **1998**, *396*, 152. (b) Tian, B. Z.; Liu, X. Y.; Tu, B.; Yu, C. Z.; Fan, J.; Wang, L. M.; Xie, S. H.; Stucky, G. D.; Zhao, D. Y. *Nat. Mater.* **2003**, *2*, 159. (c) Fan, J.; Boettcher, S. W.; Stucky, G. D. *Chem. Mater.* **2006**, *18*, 6391.

(4) (a) Lu, A. H.; Schuth, F. *Adv. Mater.* **2006**, *18*, 1793. (b) Yang, H. F.; Zhao, D. Y. *J. Mater. Chem.* **2005**, *15*, 1217.

(5) (a) Yue, W. B.; Zhou, W. Z. *Prog. Nat. Sci.* **2008**, *18*, 1329. (b) Shi, Y. F.; Guo, B. K.; Corr, S. A.; Shi, Q. H.; Hu, Y. S.; Heier, K. R.; Chen, L. Q.; Seshadri, R.; Stucky, G. D. *Nano Lett.* **2009**, *9*, 4215. (c) Tian, B. Z.; Liu, X. Y.; Yang, H. F.; Xie, S. H.; Yu, C. Z.; Bo, T.; Zhao, D. Y. *Adv. Mater.* **2003**, *15*, 1370. (d) Jiao, F.; Harrison, A.; Jumas, J. C.; Chadwick, A. V.; Kockelmann, W.; Bruce, P. G. *J. Am. Chem. Soc.* **2006**, *128*, 5468.

(6) Shi, Y. F.; Wan, Y.; Liu, R. L.; Tu, B.; Zhao, D. Y. *J. Am. Chem. Soc.* **2007**, *129*, 9522.

(7) Zhang, Y. C.; Shi, Y. F.; Liou, Y. H.; Sawvel, A. M.; Sun, X. H.; Cai, Y.; Holden, P. A.; Stucky, G. D. *J. Mater. Chem.* **2010**, *20*, 4162.

(8) Haffer, S.; Waitz, T.; Tiemann, M. *J. Phys. Chem. C* **2010**, *114*, 2075.

(9) Jiao, F.; Jumas, J. C.; Womes, M.; Chadwick, A. V.; Harrison, A.; Bruce, P. G. *J. Am. Chem. Soc.* **2006**, *128*, 12905.

(10) Kleitz, F.; Choi, S. H.; Ryoo, R. *Chem. Commun.* **2003**, 2136.

(11) Imperor-Clerc, M.; Bazin, D.; Appay, M. D.; Beaunier, P.; Davidson, A. *Chem. Mater.* **2004**, *16*, 1813.

(12) (a) Fischer, R. X.; Baur, W. H.; Shannon, R. D.; Staley, R. H.; Vega, A. J.; Abrams, L.; Prince, E. *J. Phys. Chem.* **1986**, *90*, 4414. (b) Jia, C. J.; Massiani, P.; Barthomeuf. *J. Chem. Soc., Faraday Trans.* **1993**, *89*, 3659.